Electronic Supplementary Information

Highly Efficient Platinum-Based Emitters for Warm White Light Emitting Diodes

Violeta Sicilia,* Sara Fuertes, Andrés J. Chueca, Lorenzo Arnal, Antonio Martín, Mariano Perálvarez, Chiara Botta, Umberto Giovanella,

CONTENTS

1. Experimental Details

1.1. General procedures and instrumentation. ^{1}H, $^{13}C\{^{1}H\}$, $^{31}P\{^{1}H\}$ and $^{195}Pt\{^{1}H\}$ NMR spectra were recorded on a Bruker Avance 400 and 300 MHz instrument using the standard references: $SiMe_4$ (^{1}H and ^{13}C), 85% H_3PO_4 (^{31}P), and Na_2PtCl_6 in D_2O (^{195}Pt). Coupling constant, *J* is given in Hz and assignments are based on ^{1}H-^{1}H COSY and ^{1}H-^{13}C HSQC and HMBC experiments. Infrared spectra were recorded on Perkin-Elmer Spectrum 100 FT-IR spectrometer (ATR range 250-4000 cm^{-1}) as neat solids. Mass spectra were acquired using the Microflex matrix-assisted laser desorption ionization-time-of-flight (MALDI-TOF) Bruker or an Autoflex III MALDI-TOF Bruker instruments. elemental analyses were carried out in a Perkin-Elmer 2400 CHNS analyzer. Molar conductances were carried out on a Philips PW9509 conductimeter in acetone solution (5×10^{-4} M). UV-visible spectra were registered on a Unicam UV4 spectrophotometer. Diffuse reflectance UV-vis (DRUV) spectra were recorded on a Thermo electron corporation evolution 600 spectrophotometer equipped with a Praying Mantis integrating sphere. The solid samples were homogeneously diluted with silica. The mixtures were placed in a homemade cell equipped with quartz window. Steady-state photoluminescence spectra were recorded on a Jobin-Yvon Horiba Fluorolog FL-3-11 Tau 3 spectrofluorimeter. Phosphorescence lifetimes were recorded with a Fluoromax phosphorimeter accessory containing a UV xenon flash tube. Nanosecond lifetimes were recorded with a Datastation HUB-B with a nanoLED controller and software DAS6. The nanoLEDs employed for lifetime measurements were of 340, 370, and 390 nm. The lifetime data were fitted using the Jobin-Yvon software package and the Origin Pro 8 program. Quantum yields in the solid state were measured using the Hamamatsu Absolute PL Quantum Yield Measurement System C11347-11.

1.2. X-ray structure determinations. Single crystals of **1A, 3A, 1B, 2B** and **3B** were obtained by slow diffusion of *n*-hexane (**1A** and **3B**) or diethyl ether (**3A** and **2B**) into saturated CH_2Cl_2 solutions. Those of **1B** by slow diffusion of diethyl ether into a saturated acetone solution. The crystal data, data collection parameters, and structure solution and refinement details for the crystal structures are summarized in Table S1. Crystals were mounted at the end of quartz fibres. Data collections were carried out on an Oxford Diffraction Xcalibur diffractometer using graphite monochromated MoKα radiation (0.71073 Å). The sample temperature was controlled using an Oxford Diffraction CryojetXL cooling device (100(2) K). The diffraction frames were

integrated and corrected from absorption by using the CrysAlis RED program.[1] Structure solution, followed by full-matrix least-squares refinement (all data) was performed using SHELX[2] under the WinGX package.[3] All non-hydrogen atoms were refined with anisotropic displacement parameters and refined without positional constraints, except as noted below. The solvent molecules in **1A** and **3A** are disordered and were modelled and refined with the use of geometry restrains and the use of a common set of anisotropic thermal parameters. In spite of this, all molecular complexes are well defined. For **2B**, very diffuse electron density was found in a region of the unit cell. After several unsuccessful attempts to model it as some disordered solvent, namely diethyl ether, the SQUEEZE procedure as implemented in PLATON[4] was used to deal with this electron density. For **3B**, one of the CH_2Cl_2 moieties is disordered over two positions which were refined with 0.85/0.15 partial occupancy. Soft restrains in the geometry of these were applied. The isotropic displacement parameters of all hydrogen atoms were fixed to 1.2 times the *Ueq* value of the atoms they are linked to (1.5 times for methyl groups). Full-matrix least-squares refinement of these models against *F*2 converged to final residual indices given in Table S1. CCDC Nos. 1885174-1885178 contain the supplementary crystallographic data for **1A·CH_2Cl_2**, **3A·0.5·CH_2Cl_2**, **1B·Me_2CO**, **2B** and **3B·2 CH_2Cl_2** respectively.

Table S1. Crystallographic data

	1A·CH_2Cl_2	**3A·0.5 CH_2Cl_2**	**1B·Me_2CO**	**2B**	**3B·2 CH_2Cl_2**
Empirical formula	$C_{40}H_{35}Cl_2F_6N_2P_3Pt$	$C_{44.5}H_{36}ClF_6N_2P_3Pt$	$C_{41}H_{41}F_6N_2O_3P_3Pt$	$C_{39}H_{37}F_6N_2O_2P_3Pt$	$C_{45}H_{41}Cl_4F_6N_2O_2P_3Pt$
Formula weight	1016.60	1036.20	1011.76	967.70	1185.60
Crystal system	Triclinic	Triclinic	Triclinic	Triclinic	Monoclinic
Space group	*P*-1	*P*-1	*P*-1	*P*-1	P 2_1/c
a (Å)	11.7323 (2)	10.618(5)	10.85809(11)	10.15395(15)	10.90247(13)
b (Å)	12.4706(2)	12.761(5)	13.99284(15)	14.16160(19)	25.5722(4)
c (Å)	14.5534(3)	15.582(5)	14.07706(19)	16.3056(2)	16.9913(2)
α (°)	82.239(2)	92.123(5)	93.6331(10)	70.9422(13)	90
β (°)	71.689(2)	101.549(5)	109.6815(11)	75.4245(13)	94.9749(11)
γ (°)	74.258(2)	105.048(5)	92.2688(8)	74.2959(12)	90
Volume ($Å^3$) / Z	1942.7(6) / 2	1988.8(14) / 2	2005.58(4) / 2	2098.81(6) / 2	4719.32(11) /4
ρ (Mg/m^3)	1.738	1.730	1.675	1.531	1.669
μ (Mo-Kα)/mm^{-1}	3.934	3.780	3.687	3.518	3.365
F(000)	1000	1022	1004	956	2344
Crystal size (mm)	0.41 x 0.38 x 0.18	0.40 x 0.37 x 0.15	0.50 x 0.39 x 0.29	0.42 x 0.36 x 0.27	0.45 x 0.35 x 0.24
Theta range (°)	4.43 - 30.24	4.21 - 30.24	3.34 - 30.81	3.15 - 30.17	3.18 - 30.13
Reflections collected	37872	38762	99052	51715	47053
Independent reflections [R(int)]	10281 [0.0278]	10451 [0.0411]	11124 [0.0328]	11318 [0.0356]	12540 [0.0638]
Final R_1, wR_2[a] [I>2σ(I)]	0.0227, 0.0468	0.0305, 0.0651	0.0168, 0.0385	0.0237, 0.0575	0.0376, 0.0844
R_1, wR_2[a] (all data)	0.0256, 0.0479	0.0389, 0.0685	0.0178, 0.0388	0.0265, 0.0592	0.0479, 0.0890
GOF (F^2)[b]	1.032	1.023	1.043	1.031	1.036
Largest diff. peak, hole/e.$Å^{-3}$	1.390 and - 1.217	1.505, -1.038	0.743, -0.833	0.981 and -0.931	4.214 and -1.471

[a] $R_1 = \Sigma(|F_o|-|F_c|) / \Sigma |F_o|$. $wR_2 = [\Sigma w (F_o^2-F_c^2)^2/\Sigma w(F_o^2)^2]^{1/2}$. [b] Goodness-of-fit = $[\Sigma w (F_o^2-F_c^2)^2/ (n_{obs}-n_{param})]^{1/2}$

1.3. Computational methods

Density functional calculations were performed using the M06 hybrid density functional[5] under the Gaussian09 package.[6] The SDD pseudopotential and associated basis set[7] was used for platinum, and the 6-31G(d)[8, 9] basis set was used for all other atoms. Geometry optimisations were performed under no symmetry restrictions using the initial coordinates of models derived from X-ray data. Atomic coordinates (x, y, z) for the optimized structures are listed in the Tables S4−S9. The time-dependent density-functional (TD-DFT) calculations were also carried out in the presence of dichloromethane using the polarizable continuum model (PCM) implemented Gaussian 09 package. Mulliken population analysis was carried out using Gaussian 09 package for interpretation purposes. Molekel,[10] GaussView5 and ChemissianLab program packages were used for analysis and graphic representation of molecular structures and orbitals.

1.4 Preparation of the PMMA films. For quantum yield measurements PMMA thin films were prepared by dissolving 10^{-5} mol of the complex in 1 mL of dichloromethane (10^{-2} M, 5% weight). After that, PMMA (95% weight) was slowly added with vigorous stirring. The clear solutions were deposited on optical grade quartz plates of 1x1 cm by drop casting, and allowed to dry overnight before the measurements were carried out.

1.5 OLEDs performance

For the construction of the devices ITO was used as anode. After sequential cleaning of the ITO-coated glass of 2.5 cm x 2.5 cm (ITO 2.5 cm x 0.8 cm) with water, acetone and isopropanol in a sonicator for ten minutes in each solvent at 50 ºC, it was treated with a nitrogen plasma for ten minutes. The effects of two different Hole Injection Layers (HIL) were studied: PEDOT: PSS was spin-coated to a 50 nm thickness, while MoO_3 was sublimated inside a high vacuum evaporator to a 15 nm thickness. Solutions of the different emitters with the selected bipolar matrix (PVK or TCTA, and OXD-7 or PBD) in $CHCl_3$ at a total concentration of 15 mg/mL were spin-coated on top of the anode at 2000 rpm to get the Emissive Layer (EML). Various Electron Transport Layers (ETL) were also studied in order to improve the charge balance in the device: TPBi and ZnO. While ZnO and the two different organic interlayers were spin-coated, TPBi was deposited to a 20 nm thickness using an Organic Molecular Beam Epitaxy (OMBE)

system. The chemical structures of the organic components of the devices are shown in Scheme S2.

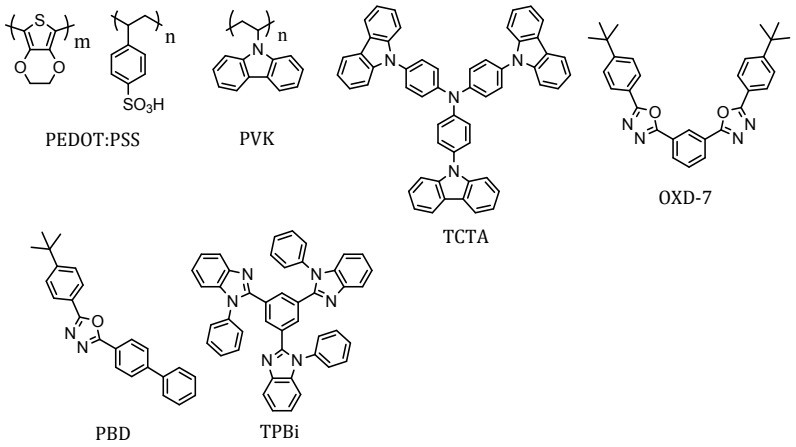

Scheme S2. Chemical structures of the different materials used in the OLEDs.

Finally 10 nm of Ba and 120 nm of Al were termosublimated inside the high vacuum evaporator to achieve a mirror cathode. Photons emitted in forward direction through the glass substrate were collected by a calibrated photodiode. Current density-Luminance-voltage curves are recorded by Keithley 2602 apparatus.

1.6 Remote phosphor devices' preparation

The deposition of the phosphors was carried out *via* screen printing using suspensions of complexes **1A**, **1B**, **3B** and [Pt(bzq)(CN)(CNXyl)] (**R**) as blue (**1B**, **3B**), orange (**1A**) and red (**R**) components on a commercial transparent terpineol based ink vehicle (fuel cell materials 311006), on top of a glass disc of 1.6 mm thick and 27 mm diameter (window). Each layer deposited contained a total weight of 1.5 mg. The different emitters were deposited in different layers with ink vehicle layers in between to avoid ligand exchange processes. The quantity of each phosphor for the desired final white light emission was determined by their individual spectra and their respective quantum efficiency. In practice, this was correlated to the number of layers of each suspension deposited and the proportion of the platinum complexes in the suspensions.

Slurries of the different emitters were prepared at different concentrations. **1A** was prepared at a 40% w/w by mixing 78.2 mg (0.084 mmol) of complex with 117.2 mg of ink vehicle. **1B** was prepared at a 40% w/w by mixing 80.0 mg (0.084 mmol) of complex with 120.0 mg of ink vehicle. For **3B,** the mixture was prepared at 40% w/w

by mixing 85.2 mg (0.084 mmol) of complex with 127.8 mg of ink vehicle. The red emitter **R** was suspended at a 10% w/w by mixing 29.7 mg (0.056 mmol) of complex with 267.0 mg of ink vehicle.

Device 1 (D1): 2 layers of **1B**, 3 layers of ink vehicle and 3 layers of **1A**.

Device 2 (D2): 2 layers of **3B**, 3 layers of ink vehicle and 3 layers of **1A**.

Device 3 (D3): 4 layers of **1B**, 3 layers of ink vehicle and 2 layers of **R**.

Device 4 (D4): 4 layers of **3B**, 3 layers of ink vehicle and 2 layers of **R**.

Device 5 (D5): 3 layers of **3B**, 3 layers of ink vehicle and 1 layers of **R**.

Device 6 (D6): 4 layers of **3B**, 3 layers of ink vehicle and 1 layers of **R**.

Device 7 (D7): 2 layers of **3B**, 3 layers of ink vehicle and 4 layers of **R**.

Device 8 (D8): 2 layers of **3B**, 3 layers of ink vehicle and 3 layers of **R**.

Device 9 (D9): 3 layers of **1B**, 3 layers of ink vehicle and 1 layers of **R**.

Device 10 (D10): 4 layers of **1B**, 3 layers of ink vehicle and 1 layers of **R**.

2.- $^{31}P\{^{1}H\}$, $^{195}Pt\{^{1}H\}$ NMR spectra

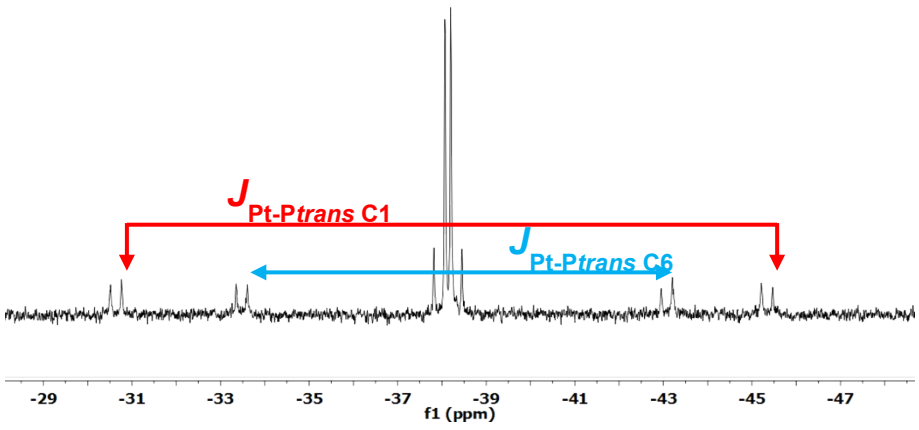

Figure S1: $^{31}P\{^{1}H\}$ NMR spectrum of **1B** in CD_2Cl_2, AB system

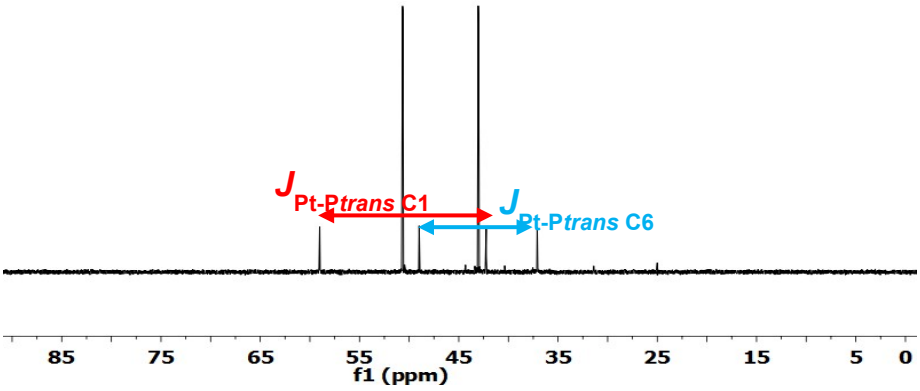

Figure S2: $^{31}P\{^{1}H\}$ NMR spectrum of **2A** in CD_2Cl_2

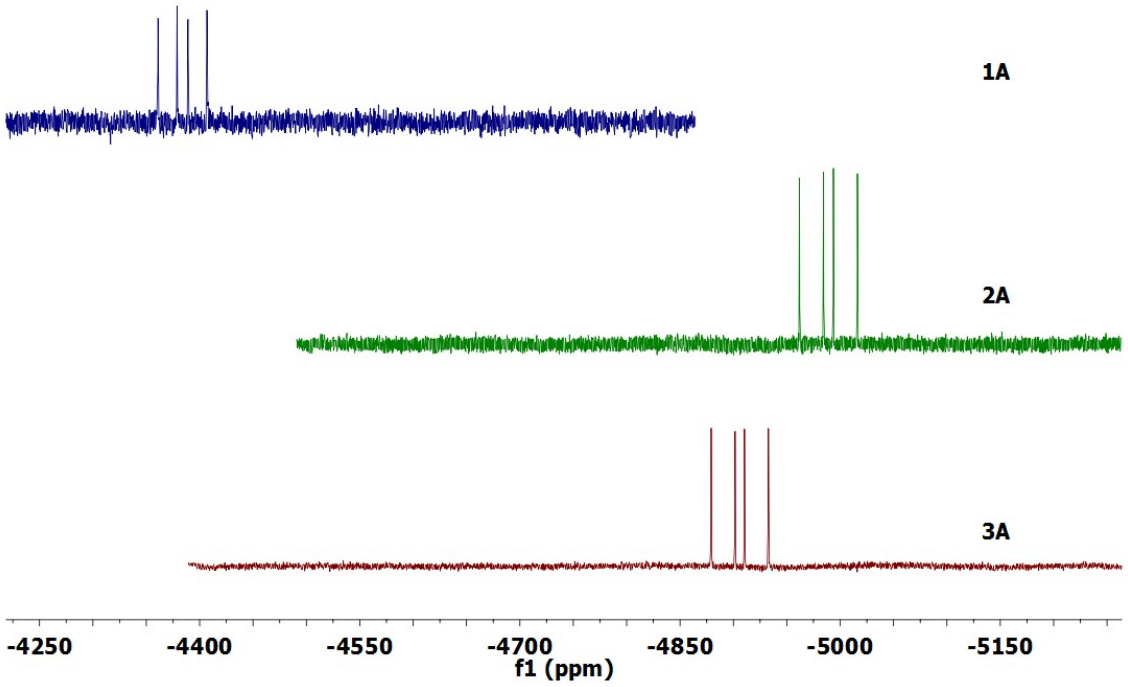

(a)

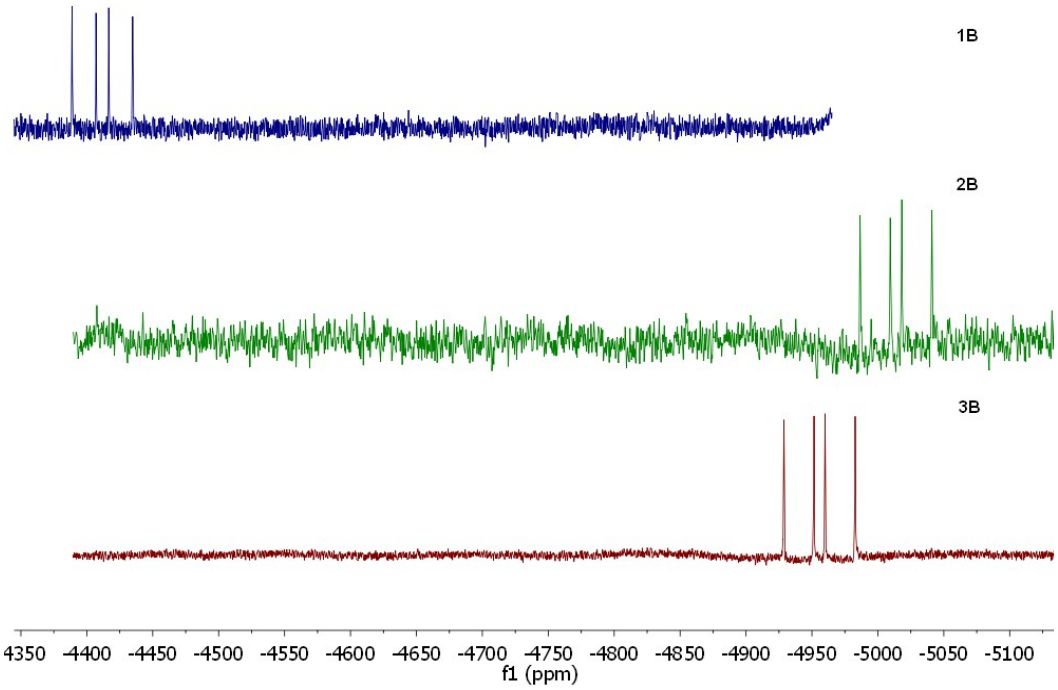

(b)

Figure S3: $^{195}Pt\{^{1}H\}$ NMR spectra of **1A-3A** (a) and **1B-3B** (b) in CD_2Cl_2

3. X-ray molecular structures

The X-ray diffraction study on single crystals of **1A**, **3A** and **1B, 2B, 3B** (Figure S4 and Table S2) confirmed that in all of these complexes the platinum center exhibits a distorted square-planar environment as a consequence of the small bite angles of both chelate ligands (R-C^C* and P^P, especially when P^P is dppm). Bond distances and angles concerning the "Pt(C^C*)" moiety are similar to those observed for other five-membered metalacycles of Pt(II) with the N-heterocyclic carbenes.[11-15] Regarding the "Pt(P^P)" fragment, the Pt–P1 bond lengths [2.3209(6) - 2.3088(9) Å] are slightly longer than those of the Pt-P2 ones [2.2886(10) - 2.2765(9) Å], complying with the C6 atom having a higher *trans* influence than that of the C1 atom.[12] The P-Pt-P bite angles in **2B** and **3B** are rather similar (~ 84°). However, this bite angle in **1A** (71.72º) and **1B** (72.88°) are significantly smaller than 90°, implying that the four-membered chelate ring is under great strain. The chelating dppe ligand adopts the gauche conformation with P1-C38-C39-P2 torsion angles of 54.87°. In the cation complexes of **3A** and **3B** the benzene ring (C38-C43) are not coplanar with the Pt (II) coordination plane (Pt, C1, C6, P1, P2), forming a dihedral angle of 18.99º and 15.86°, respectively.

In their crystal structure packings, there are no Pt-Pt contacts. However, rather weak intermolecular interactions were observed. The molecules arrange themselves in pairs in a head-to-tail fashion supported by π···π (3.49 – 3.37 Å) intermolecular contacts between the C^C* fragments, see Figure S5a as an example. Also, in all five crystal structures there are some weak C-H···F contacts (d C-F= 2.97 - 3.32 Å; d H-F= 2.33 - 2.85 Å) between the complex cation and the PF_6^- anion (see Figure S5b as an example).[16-18]

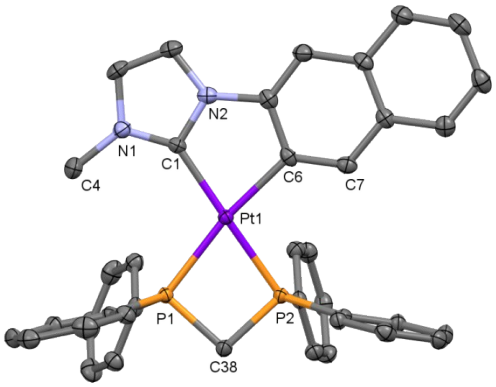

(a)

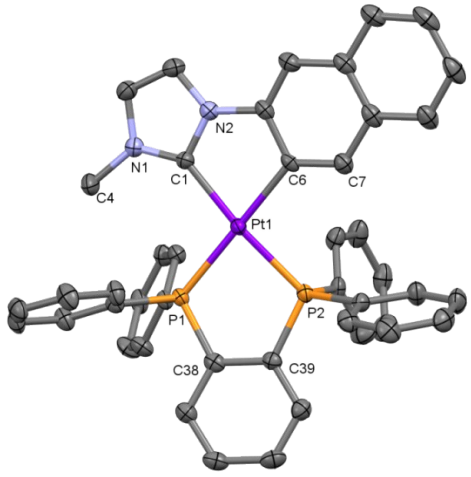

(b)

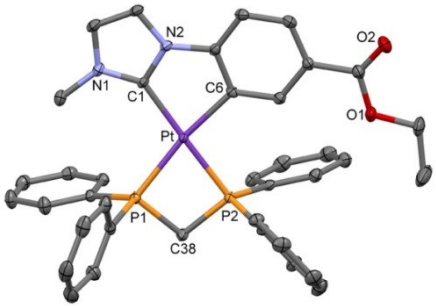

(c)

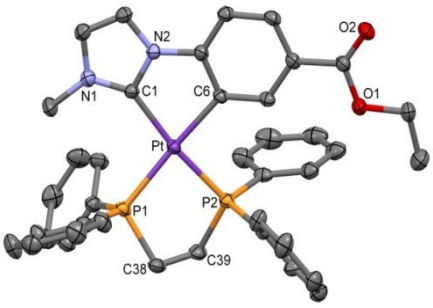

(d)

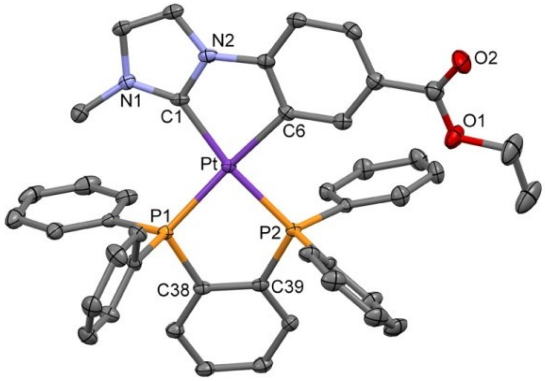

(e)

Figure S4: Molecular structures of the cation complexes **1A** (a) and **3A** (b), **1B** (c), **2B** (d) and **3B** (e). Thermal ellipsoids are drawn at the 50% probability level. Hydrogen atoms, PF_6 and solvent molecules have been omitted for clarity.

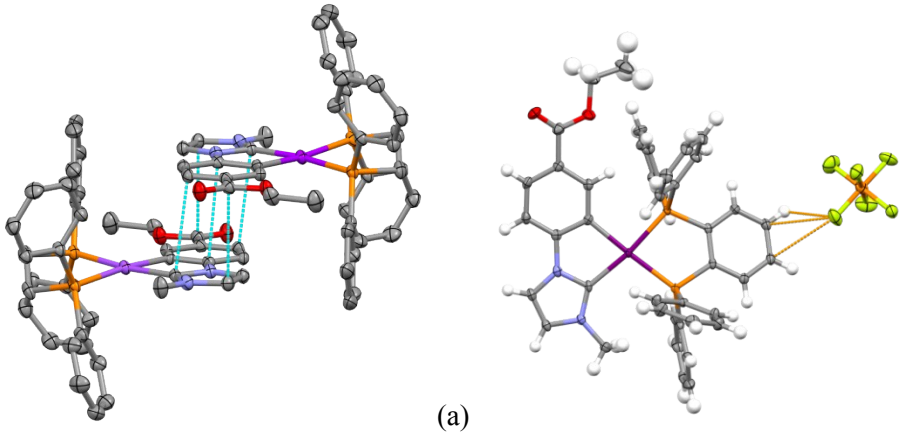

(a) (b)

Figure S5: (a) Crystal packing view of **2B**. (b) Molecular structure of **3B** showing C···H-F intermolecular contacts.

Table S2: Selected bond lengths (Å) and angles (°)**.**

	1A·CH_2Cl_2	**3A·0.5 CH_2Cl_2**	**1B·Me_2CO**	**2B**	**3B·2 CH_2Cl_2**
Pt(1)-C(1)	2.030(2)	2.0602(3)	2.0389(14)	2.061(2)	2.060(4)
Pt(1)-C(6)	2.047(2)	2.086(3)	2.0550(15)	2.074(2)	2.072(3)
Pt(1)-P(1)	2.3209(6)	2.3020(11)	2.3121(4)	2.3119(6)	2.3088(9)
Pt(1)-P(2)	2.2831(6)	2.2886(10)	2.2877(4)	2.2819(6)	2.2765(9)
C(1)-Pt(1)-C(6)	79.66(9)	79.30(12)	78.92(6)	79.38(8)	78.89(15)
C(6)-Pt(1)-P(2)	100.08(7)	97.55(9)	100.43(4)	94.33(6)	93.70(11)
C(1)-Pt(1)-P(1)	108.65(6)	100.66(9)	108.02(4)	102.04(6)	103.33(10)
P(1)-Pt(1)-P(2)	71.72(2)	82.83(3)	72.882(14)	84.67(2)	84.76(3)

Some degree of cation-anion association seems to occur in acetone solutions, which substantiates the low conductivity values observed for them (Λ_M: 62.9-68.4 Ω^{-1} cm^2 mol^{-1} in a $5 \cdot 10^{-4}$ M acetone solution) compared with the expected ones (100-120 Ω^{-1} cm^2 mol^{-1}).[19]

4. Absorption data and spectra

Table S3: Absorption Data in $5 \cdot 10^{-5}$ M solutions for **1A-3A** and **1B-3B** at 298 K.

Comp	λ abs /nm (10^3 ε M^{-1} cm^{-1})
1A	232 (58.7), 269 (22.9), 277 (25.0), 285 (25.7), 296 (25.4), 322 (4.3), 328 (4.5), 353 (5.1), 368 (4.8) tail to 390 ***CH_2Cl_2***
	229 (57.5), 269 (26.1), 277 (28.8), 284 (29.9), 296 (28.9), 323 (5.3), 327 (5.1), 351 (5.2), 366 (4.8) tail to 390 ***THF***
	227 (76.2), 269 (31.8), 277 (34.9), 283 (35.7), 293 (32.8), 320 (6.3), 326 (6.3), 347 (5.7), 360 (5.1) tail to 390 ***MeCN***
	226 (67.4), 269 (27.0), 276 (29.2), 283 (30.4), 294 (28.8), 322 (4.8), 327 (4.8), 350 (5.0), 364 (4.6) tail to 390 ***MeOH***
	294, 329, 349, 365 ***Solid***
2A	232 (61.1), 253 (30.3), 269 (27.9), 276 (30.3), 290 (32.8), 318 (6.7), 331 (4.6), 348 (4.6), 364 (4.2) tail to 390 ***CH_2Cl_2***
	227 (47.7), 253 (22.7), 269 (23.6), 277 (26.0), 290 (27.9), 318 (5.7), 331 (3.9), 346 (3.7), 363 (3.1) tail to 390 ***THF***
	224 (70.1), 252 (29.5), 269 (28.3), 275 (30.8), 288 (32.3), 318 (6.4), 328 (4.8), 342 (4.1), 359 (3.2) tail to 390 ***MeCN***
	224 (70.9), 252 (29.3), 268 (28.8), 275 (31.9), 288 (33.3), 317 (6.5), 331 (4.4), 345 (4.3), 362 (3.6) tail to 390 ***MeOH***
	295, 322, 345, 360 ***Solid***
3A	233 (69.1), 269 (322), 277 (32.2), 287 (30.4), 299 (26.7), 317 (7.1), 331 (4.8), 347 (4.9), 364 (4.6) tail to 390 ***CH_2Cl_2***
	232 (63.0), 269 (30.6), 277 (30.6), 286 (29.0), 298 (25.2), 317 (7.0), 333 (4.5), 348 (4.6), 363 (4.1) tail to 390 ***THF***
	226 (77.7), 269 (32.9), 276 (33.3), 285 (31.8), 294 (28.1), 316 (7.8), 330 (5.2), 343 (4.9), 359 (3.9) tail to 390 ***MeCN***
	226 (74.9), 269 (31.7), 276 (31.9), 285 (30.4), 295 (26.6), 316 (7.3), 330 (4.7), 346 (4.6), 362 (4.0) tail to 390 ***MeOH***
	285, 302, 324, 345, 366 ***Solid***

1B	227 (63.2), 231 (57.5), 261 (35.9), 309 (6.4), 324 (7.0), 347 (2.2) tail to 380 ***CH_2Cl_2*** 232 (42.4), 236 (45.9), 261 (32.0), 308 (5.6), 323 (6.0), 346 (1.8) tail to 380 ***THF*** 228 (55.6), 260 (34.1), 306 (6.9), 322 (7.1), 347 (2.2) tail to 380 ***MeCN*** 228 (55.5), 261 (32.9), 308 (5.8), 323 (6.3), 346 (1.9) tail to 380 ***MeOH*** 242, 272, 322, 348, tail to 400 ***Solid***
2B	230 (45.1), 261 (31.7), 306 (4.8), 320 (5.5), tail to 380 ***CH_2Cl_2*** 234 (39.7), 262 (32.9), 305 (5.1), 320 (5.8), tail to 380 ***THF*** 222 (46.8), 261 (28.9), 305 (5.1), 318 (5.4), tail to 380 ***MeCN*** 222 (52.8), 262 (31.9), 305 (5.2), 319 (5.7), tail to 380 ***MeOH*** 231, 271, 318, tail to 400 ***Solid***
3B	234 (67.6), 262 (37.6), 305 (9.1), 319 (9.5), tail to 380 ***CH_2Cl_2*** 238 (48.6), 262 (31.1), 306 (5.8), 320 (6.5), tail to 380 ***THF*** 229 (58.5), 261 (32.3), 305 (6.4), 319 (6.9), tail to 380 ***MeCN*** 228 (51.0), 262 (28.1), 305 (5.3), 319 (5.8), tail to 380 ***MeOH*** 243, 273, 317, tail to 400 ***Solid***

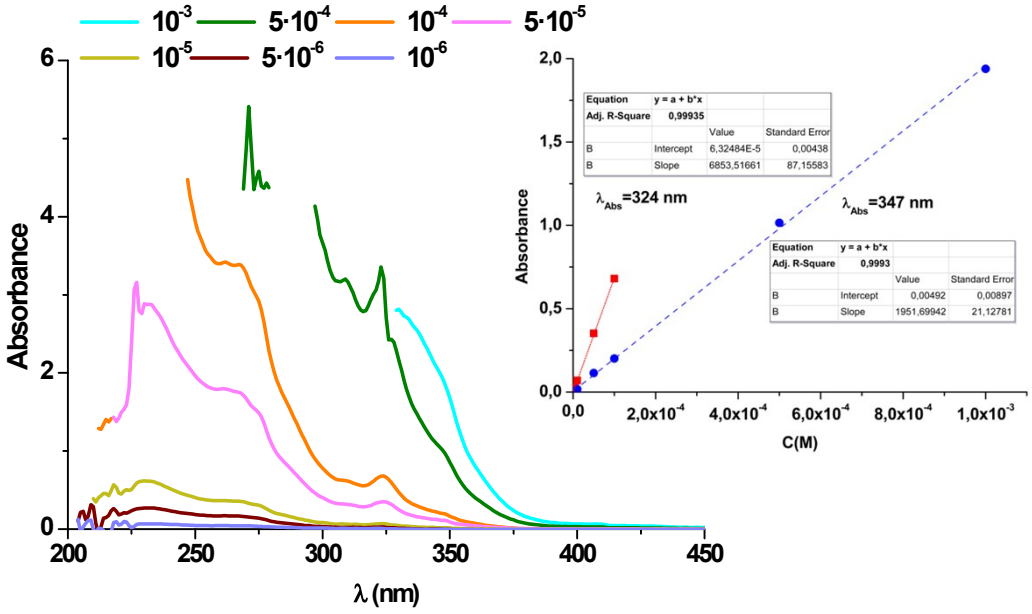

Figure S6: UV-Vis absorption spectra of **1B** in CH_2Cl_2 at several concentrations (M) at r.t. Insets: Linear fit representation of the absorbance vs concentration.

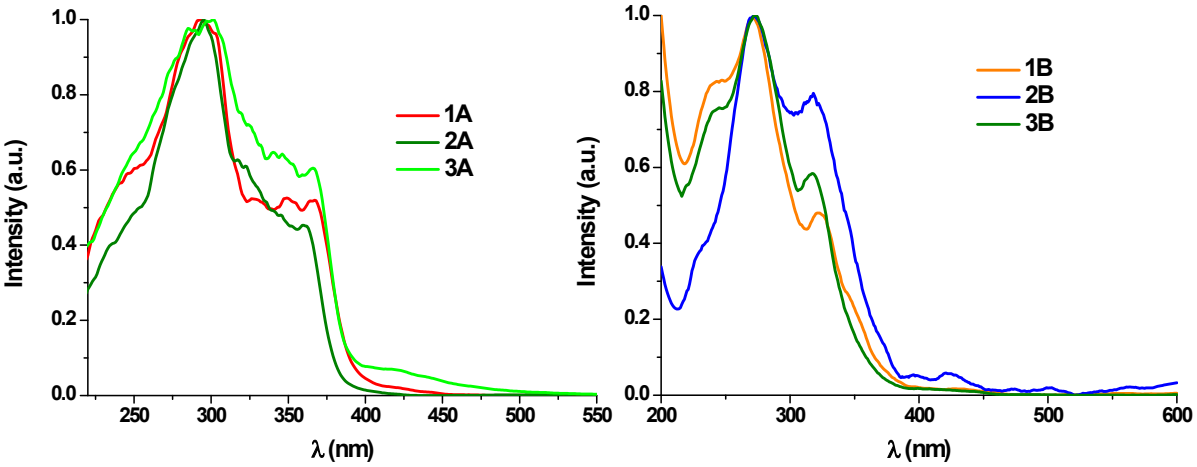

Figure S7: Normalized diffuse reflectance spectra of **1A-3A** (left) **1B-3B** (right) of powdered samples at r.t.

5. DFT and TD-DFT Studies on 1A, 3A, 1B and 3B

The geometric parameters of the optimized structures agree well with the experimental values (Table S4-S9). The calculated excited states, S_1, in CH_2Cl_2 are listed in Table S9 and represented in Figures S8-S11 together with the molecular orbitals involved; their relative compositions are reported in Table S8. The lowest energy calculated absorptions (S_1) fit well with the experimental absorptions, also reproducing the observed red shift of the dppm derivatives in relation to the dppbz ones. The main contribution to the S_1 is the HOMO → LUMO transition with a small partipation of the HOMO-1 → LUMO in **1A** and **3A** (see Table S9). Analyses of the frontier orbitals indicate that the highest occupied molecular orbital (HOMO) is primarily centered on the C^C* ligand (89% **1A**, 93% **3A**, 78% **1B** and 80% **3B**) and to a minor extent on the Pt center (6% **1A**, 5% **3A**, 21% **1B** and 18% **3B**). In fact, in compounds **1A** and **3A**, the HOMO is almost entirely localized on the naphthyl system (~ 90%). By contrast, the lowest unoccupied molecular orbital (LUMO) is allocated on the C^C* ligand (38% **1A**, 33% **3A**, 53% **1B** and 51% **3B**), Pt (29% **1A**, 24% **3A**, 24% **1B** and 21% **3B**) and the P^P ligands (33% **1A**, 43% **3A**, 23% **1B** and 28% **3B**). As noticed, the LUMO is approximately equally distributed over the three fragments with subtle differences. In **1B** and **3B,** the contribution of the C^C* fragment is bigger and that of the P^P fragment is lower than those in the naphthyl derivatives, (**1A** and **3A**).

Table S4: DFT-Optimized coordinates of **1A** in the Ground State.

Center	Coordinates (Angstroms)			Center	Coordinates (Angstroms)		
	X	Y	Z		X	Y	Z
Pt	-0.034255	-0.611853	-0.075763	H	-2.914477	0.960387	0.193369
P	2.233800	0.018232	0.408349	C	3.300464	-0.996024	1.476092
P	0.011158	1.635530	0.645712	C	0.884893	5.007179	-1.511954
C	-0.042736	-2.570533	-0.664172	H	1.421670	5.941905	-1.363747
N	-1.266455	-3.094842	-0.943047	C	-1.410653	1.418183	2.997755
N	0.831018	-3.572141	-0.890834	H	-0.956633	0.425921	3.050658
C	-2.054072	-0.933492	-0.344075	C	-2.284415	1.835547	3.993015
C	1.704583	1.506177	1.396052	H	-2.502305	1.179706	4.833403
H	1.594314	1.211412	2.449105	C	0.265804	4.740756	-2.731905
H	2.347795	2.393538	1.343601	H	0.323852	5.469523	-3.538001
C	2.859685	0.374448	-2.267260	C	3.583881	0.894551	-3.336059
H	1.985450	-0.254283	-2.446807	H	3.286942	0.662700	-4.356822
C	0.126735	2.874634	-0.670586	C	-2.892066	3.087282	3.904142
C	-2.395800	-2.250182	-0.782562	H	-3.583044	3.410880	4.680091
C	2.704930	-1.565329	2.609442	C	-6.092883	-2.125747	-1.049075
H	1.661607	-1.345397	2.847118	H	-6.310194	-3.139397	-1.386822
C	-0.491268	2.610796	-1.896709	C	-1.741221	3.511218	1.826187
H	-1.016008	1.665585	-2.042668	H	-1.533861	4.166267	0.980880
C	0.817387	4.077109	-0.481707	C	-5.522137	0.470154	-0.177720
H	1.295134	4.293893	0.474489	H	-5.292730	1.479794	0.165088
C	-7.109950	-1.223461	-0.846083	C	3.430381	-2.429846	3.419083
H	-8.142786	-1.517230	-1.024479	H	2.963844	-2.867115	4.299564
C	-1.125447	2.261452	1.916654	C	0.159426	-4.712053	-1.305016
C	2.270596	-3.494399	-0.701174	H	0.685487	-5.627851	-1.538232
H	2.673647	-2.632986	-1.243730	C	-2.624388	3.919775	2.822412
H	2.724267	-4.404659	-1.099884	H	-3.103475	4.894114	2.749950
H	2.512538	-3.406633	0.363954	C	-1.162210	-4.412355	-1.339042
C	-6.822392	0.086353	-0.405649	H	-2.015671	-5.016620	-1.612149
H	-7.635093	0.792832	-0.246520	C	-3.675164	-2.666769	-1.019586
C	3.235875	0.673995	-0.954492	H	-3.896961	-3.680897	-1.353051
C	-3.098970	-0.060204	-0.153348	C	4.748492	-2.745911	3.093345

H	5.314603	-3.429903	3.722436	H	5.249751	2.119435	-3.931107
C	-4.453871	-0.434200	-0.380583	C	4.338399	1.504957	-0.718779
C	-4.746353	-1.757314	-0.822724	H	4.634214	1.748414	0.302652
C	4.618899	-1.318983	1.150775	C	-0.421248	3.545525	-2.924725
H	5.085095	-0.898541	0.260458	H	-0.900607	3.338488	-3.879359
C	5.338880	-2.193445	1.961152	C	5.061251	2.017708	-1.788458
H	6.366246	-2.443240	1.703507	H	5.919092	2.660888	-1.603397
C	4.683991	1.711788	-3.095625				

Table S5: DFT-Optimized coordinates of **3A** in the Ground State.

Center	Coordinates (Angstroms)			Center	Coordinates (Angstroms)		
	X	Y	Z		X	Y	Z
Pt	0.161625	-0.664491	0.073526	C	-1.098875	3.557116	1.248682
P	0.237760	1.652403	-0.355105	C	-3.290275	2.503502	-3.202423
P	-2.157761	-0.247715	-0.332419	C	-2.085961	-3.633628	1.025676
C	2.209752	-1.010932	0.263446	C	7.288569	-1.460632	0.282548
C	-1.139318	2.044424	-1.492135	C	0.062508	-4.874388	1.022921
C	0.192930	-2.682244	0.529830	C	0.640266	2.258179	2.317649
N	-0.646489	-3.697165	0.839003	C	1.372166	-4.589797	0.840163
C	-2.224745	1.157429	-1.507205	C	6.268196	-2.377759	0.368700
C	-3.076250	0.342838	1.129811	C	-2.582189	-2.226558	-2.202927
N	1.432897	-3.243883	0.544818	C	0.395539	2.917241	3.516119
C	-0.102794	2.580351	1.175005	C	3.837447	-2.866304	0.439395
C	3.271980	-0.136933	0.213451	C	2.165063	1.846784	-2.324063
C	1.688017	2.419461	-1.138437	C	4.918771	-1.954921	0.351323
C	2.555595	-2.390862	0.402739	C	3.502887	4.008781	-1.182494
C	-4.853330	1.620194	2.157830	C	-0.598979	3.891022	3.584937
C	-2.611386	-0.014181	2.400683	C	-3.297671	-3.217939	-2.863943
C	-3.296170	1.387468	-2.370260	C	7.002011	-0.082071	0.174995
C	-3.271970	0.432912	3.540803	C	4.627699	-0.566049	0.247401
C	-4.199239	1.170510	1.016515	C	2.355909	3.505509	-0.571594
C	-5.198459	-2.800476	-1.434918	C	-2.220467	3.393757	-3.173552
C	-1.143683	3.166054	-2.321297	C	-1.343612	4.210264	2.453800
C	5.698527	0.354057	0.158533	C	-4.605066	-3.508185	-2.476062
C	-4.487214	-1.802765	-0.772478	C	-3.174934	-1.516676	-1.152193

C	3.978733	3.432567	-2.355558	H	1.408075	1.484319	2.267410
C	3.305777	2.354216	-2.930139	H	2.246959	-5.220527	0.905524
C	-4.391107	1.250902	3.418908	H	6.484285	-3.443334	0.449801
H	3.114002	0.937856	0.126644	H	-1.553275	-2.006607	-2.495445
H	-5.723976	2.265829	2.062420	H	0.977240	2.664636	4.400461
H	-1.715797	-0.629879	2.498684	H	4.052791	-3.930221	0.538823
H	-4.132472	0.688804	-2.405587	H	1.651552	0.988197	-2.760969
H	-2.903134	0.150981	4.524934	H	4.024448	4.852870	-0.735773
H	-4.560683	1.475967	0.034354	H	-0.794856	4.400904	4.526315
H	-6.219597	-3.025709	-1.133739	H	-2.832451	-3.769642	-3.678337
H	-0.299905	3.856028	-2.312087	H	7.818589	0.634121	0.102451
H	5.465358	1.416493	0.067643	H	1.991122	3.953973	0.351786
H	-4.953808	-1.258295	0.048441	H	-2.217828	4.264416	-3.825785
H	-1.693585	3.805541	0.369555	H	-2.121889	4.968933	2.507503
H	-4.122833	2.674834	-3.881421	H	-5.161405	-4.290976	-2.987915
H	-2.376738	-2.614229	1.287750	H	4.879088	3.822995	-2.825982
H	-2.359933	-4.294136	1.853239	H	3.678030	1.904476	-3.848350
H	-2.612209	-3.946731	0.118165	H	-4.902815	1.608180	4.310475
H	8.324260	-1.795474	0.294720				
H	-0.436067	-5.800743	1.274281				

Table S6: DFT-Optimized coordinates of **1B** in the Ground State.

Center	Coordinates (Angstroms)			Center	Coordinates (Angstroms)		
	X	Y	Z		X	Y	Z
Pt	-0.422378	0.776758	-0.090417	C	-3.610327	-0.087910	1.573586
P	2.300367	-0.625186	0.434226	C	2.629013	1.316611	-0.350585
P	0.384869	-1.337461	0.606049	C	5.113928	1.588268	-0.560512
N	-2.299885	3.225098	-0.906579	C	-3.050611	-1.549711	-0.932828
N	-0.173464	3.498958	-1.082515	C	1.180920	3.089528	-0.978146
O	6.120652	2.232639	-0.774442	C	-0.747509	4.685778	-1.490774
O	5.124699	0.308512	-0.162940	C	-2.087189	4.512270	-1.379037
C	3.538681	3.396661	-1.188910	C	-1.239128	-1.871903	1.326636
C	2.249271	3.901985	-1.329230	C	1.329033	1.781655	-0.483824
C	-1.125101	2.594641	-0.720226	C	1.651949	-1.525896	1.892629

C	3.732702	2.105056	-0.702723	H	-1.518936	-2.930204	1.244884
C	0.836243	-2.491964	-0.724108	H	-1.208167	-1.603980	2.392790
C	-3.610770	2.654719	-0.635233	H	-3.730058	1.712464	-1.180455
C	6.407699	-0.296684	0.049283	H	-4.374483	3.357106	-0.976872
C	6.150860	-1.711062	0.497825	H	-3.736869	2.478910	0.438988
C	-0.080691	-3.391879	-1.272980	H	6.982085	-0.250699	-0.884841
C	2.127631	-2.408039	-1.264084	H	6.952279	0.287203	0.802471
C	2.493135	-3.221520	-2.328965	H	5.632742	-2.281245	-0.283445
C	0.290017	-4.200573	-2.343965	H	5.527667	-1.721187	1.401715
C	1.573980	-4.117568	-2.871352	H	7.096349	-2.217263	0.722541
C	-4.970587	-0.222246	1.288405	H	2.858026	-1.711581	-0.847549
C	-3.206000	0.606361	2.721128	H	-1.094537	-3.468652	-0.881586
C	-4.154239	1.136807	3.586257	H	3.499558	-3.153460	-2.737461
C	-5.916780	0.318521	2.155249	H	-0.431651	-4.899420	-2.762670
C	-5.511617	0.993389	3.302233	H	1.860970	-4.750678	-3.708559
C	1.981102	-0.421503	2.684372	H	-5.296167	-0.739310	0.386480
C	2.250955	-2.766450	2.137897	H	-2.142858	0.749345	2.927316
C	2.905714	-0.557988	3.715030	H	-6.975910	0.211892	1.929433
C	3.170044	-2.897706	3.172281	H	-3.834941	1.673370	4.477367
C	3.498277	-1.794239	3.958011	H	-6.254331	1.415947	3.975955
C	-2.758650	-1.163564	-2.244105	H	1.517271	0.546053	2.484455
C	-3.809747	-2.703944	-0.698048	H	2.000017	-3.627679	1.518653
C	-3.214186	-1.929415	-3.313577	H	3.167042	0.303964	4.325439
C	-4.263025	-3.464370	-1.768720	H	3.634625	-3.863079	3.363028
C	-3.960790	-3.078850	-3.074882	H	4.223569	-1.899448	4.762572
H	4.404220	3.999099	-1.455202	H	-2.148901	-0.275805	-2.422471
H	2.092349	4.910050	-1.708773	H	-4.037679	-3.012288	0.323339
H	2.815575	0.327325	0.059936	H	-2.977536	-1.632364	-4.333094
H	-0.171089	5.539006	-1.819563	H	-4.848941	-4.362580	-1.585341
H	-2.908625	5.182653	-1.591492	H	-4.309295	-3.682062	-3.910896

Table S7: DFT-Optimized coordinates of **3B** in the Ground State.

Center	Coordinates (Angstroms)			Center	Coordinates (Angstroms)		
	X	Y	Z		X	Y	Z
Pt	-0.374195	0.780722	0.088227	H	5.547251	-2.060860	1.530928
P	-2.362933	-0.522110	0.004475	C	-2.938432	-1.006947	1.668898
P	0.663238	-1.254944	-0.460842	C	-2.578382	-0.200483	2.755704
N	-2.173648	3.452189	0.475615	H	-1.956281	0.681928	2.594780
N	-0.047833	3.672376	0.269238	C	-2.992819	-0.528727	4.042713
O	5.208829	0.289281	0.499937	H	-2.705017	0.102786	4.880831
O	6.213758	2.302274	0.489998	C	-3.763924	-1.667197	4.255925
C	-1.038086	2.735094	0.331917	H	-4.083328	-1.927173	5.263196
C	-1.896577	4.810951	0.487969	C	-4.119199	-2.479783	3.181988
H	-2.680034	5.548769	0.594852	H	-4.715204	-3.374860	3.347616
C	-0.556818	4.950620	0.361352	C	-3.707942	-2.154449	1.894445
H	0.061249	5.836754	0.339411	H	-3.983081	-2.805660	1.065453
C	-3.523990	2.933173	0.615147	C	-3.816055	0.074658	-0.919598
H	-3.493294	1.969955	1.129537	C	-5.120700	0.008609	-0.428790
H	-3.998036	2.814621	-0.364735	H	-5.317668	-0.424460	0.552075
H	-4.106663	3.632688	1.220375	C	-6.174101	0.513266	-1.188009
C	1.293996	3.221215	0.239443	H	-7.189508	0.464723	-0.799753
C	1.417879	1.822822	0.224583	C	-5.928873	1.078403	-2.435913
C	2.712726	1.329153	0.322060	H	-6.753756	1.474735	-3.024607
H	2.891625	0.259209	0.376220	C	-4.627493	1.139095	-2.932494
C	3.829068	2.174581	0.367752	H	-4.434747	1.581313	-3.907946
C	3.656383	3.556753	0.328203	C	-3.572885	0.642576	-2.176064
H	4.531108	4.202590	0.353794	H	-2.551151	0.704645	-2.557845
C	2.375045	4.092553	0.276453	C	1.564592	-2.096040	0.880668
H	2.234672	5.171759	0.274259	C	2.349212	-3.235050	0.657464
C	5.203535	1.629136	0.456248	H	2.478777	-3.633478	-0.348282
C	6.486859	-0.350719	0.620256	C	2.984200	-3.863967	1.721383
H	6.989391	0.031622	1.517815	H	3.594217	-4.746325	1.538660
H	7.102546	-0.078008	-0.246886	C	2.842776	-3.363833	3.014539
C	6.229314	-1.832467	0.701454	H	3.343305	-3.858276	3.844850
H	7.168351	-2.373009	0.865096	C	2.064140	-2.234013	3.244493
H	5.777907	-2.209250	-0.226171	H	1.953181	-1.839785	4.252495

C	1.425898	-1.601392	2.182250
H	0.820840	-0.710879	2.361064
C	1.785323	-1.114340	-1.891394
C	1.212206	-0.790500	-3.127856
H	0.127268	-0.719857	-3.225796
C	2.020242	-0.557296	-4.233588
H	1.566403	-0.312348	-5.191803
C	3.407088	-0.632349	-4.113261
H	4.038656	-0.441347	-4.978552
C	3.981504	-0.945961	-2.886112
H	5.064419	-1.001403	-2.783544
C	3.175082	-1.189922	-1.778184
H	3.644378	-1.422465	-0.823145
C	-1.965198	-2.090418	-0.860225
C	-0.618632	-2.428333	-1.043267
C	-0.283892	-3.614615	-1.701610
H	0.760270	-3.866172	-1.883817
C	-1.281962	-4.462272	-2.164787
H	-1.014224	-5.381497	-2.681236
C	-2.622060	-4.120855	-1.994769
H	-3.403721	-4.773599	-2.377308
C	-2.963247	-2.935452	-1.355397
H	-4.012632	-2.653949	-1.263501

Table S8: Population Analysis (%) of Frontier MOs in the Ground State for **1A**, **3A**, **1B** and **3B** in solution of CH_2Cl_2

FO	eV				Pt				Ar (R–C)				Im (C*)				P^P			
	1A	**3A**	**1B**	**3B**	**1A**	**3A**	**1B**	**3B**	**1A**	**3A**	**1B**	**3B**	**1A**	**3A**	**1B**	**3B**	**1A**	**3A**	**1B**	**3B**
L	-1.87	-1.82	-2.13	-2.05	29	24	24	21	14	14	29	28	24	19	24	23	33	43	23	28
H	-6.34	-6.31	-6.80	-6.82	6	5	21	18	87	91	53	56	2	2	25	24	5	2	1	2
H-1	-6.63	-6.64	-7.24	-7.22	13	12	40	44	51	68	17	14	21	19	2	2	15	1	41	40

Table S9: Selected singlet excited states calculated by TD-DFT for **1A**, **3A**, **1B** and **3B** in solution of CH_2Cl_2

Compound	**λ_{exc} (calc.)/nm**	**o.s.**	**Transition (% contribution)***	**Assignment**
1A	346.0	0.1523	HOMO → LUMO (71); H-1 → L (20)	LL'CT, LMCT, ILCT
3A	339.5	0.1612	HOMO → LUMO (80); H-1 → L (6)	LL'CT, LMCT, ILCT
1B	351.6	0.0017	HOMO → LUMO (97)	ILCT, LL'CT
3B	338.4	0.0033	HOMO → LUMO (95)	ILCT, LL'CT

* Transitions with contributions < 5% were not included

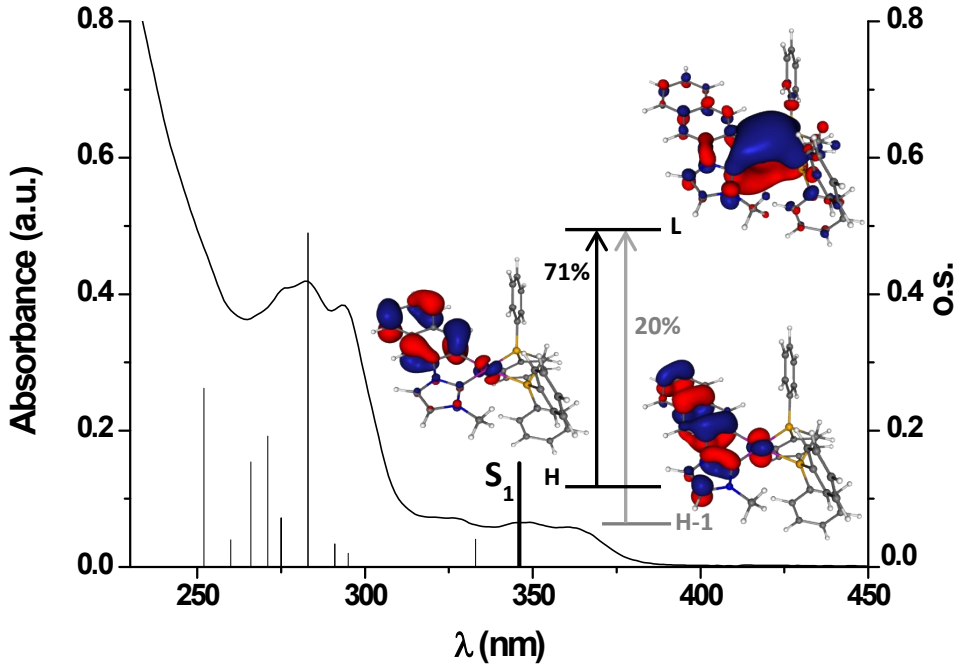

Figure S8: Normalized UV-vis absorption spectrum, calculated transitions in CH_2Cl_2 (bars) and calculated molecular orbitals for compound **1A.**

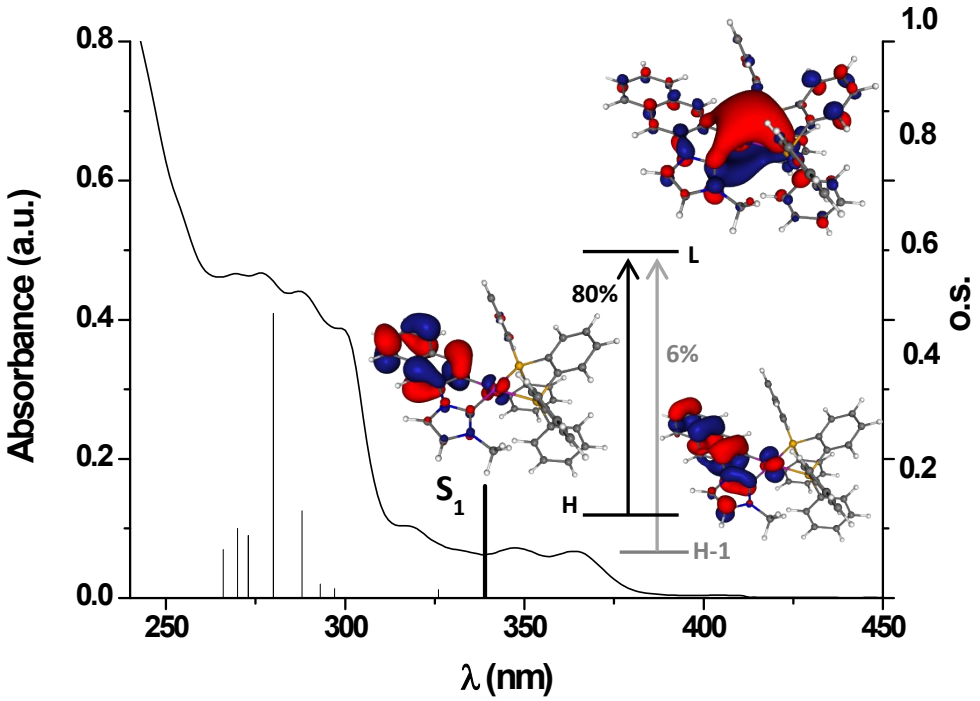

Figure S9: Normalized UV-vis absorption spectrum, calculated transitions in CH_2Cl_2 (bars) and calculated molecular orbitals for compound **3A.**

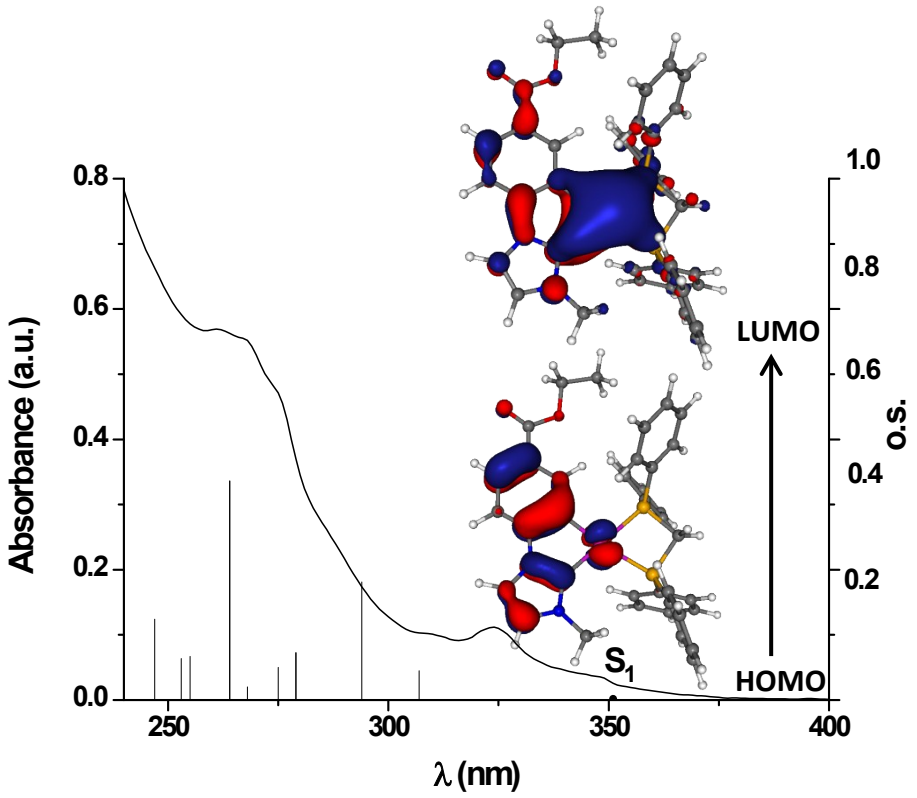

Figure S10: Normalized UV-vis absorption spectrum, calculated transitions in CH_2Cl_2 (bars) and calculated molecular orbitals for compound **1B.**

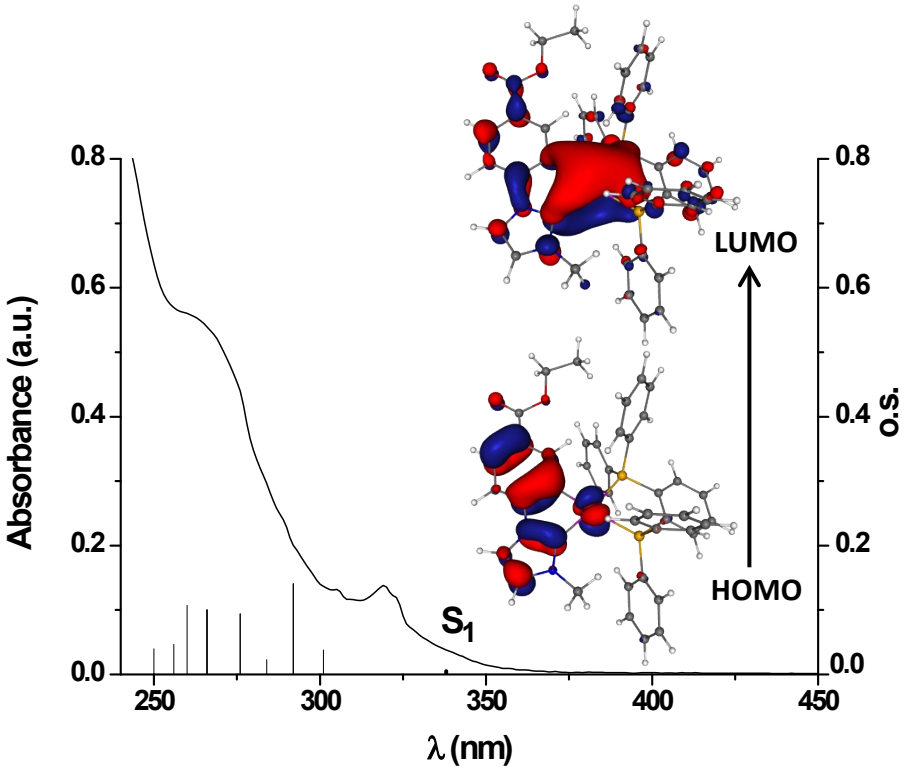

Figure S11: Normalized UV-vis absorption spectrum, calculated transitions in CH_2Cl_2 (bars) and calculated molecular orbitals for compound **3B.**

6. Emission spectra and data

Table S10: Emission data for 1A–3A and 1B–3B .

Comp.	Media (T/K)	λ_{ex} (nm)	λ_{em} (nm)	τ (μs)[c]	ϕ[d]
1A	CH_2Cl_2[a](77)	367	470_{max}, 505, 546, 598_{sh}	286.1	
	CH_2Cl_2[b] (77)	380	473_{max}, 509, 556, 606, 656_{sh}	211.0	
		418	473, 509, 560_{max}, 608, 658_{sh}	72.5	
	PMMA Film	340	473_{max}, 508, 547, 592_{sh}		0.75
	Solid (298)	400	560, 605_{max}, 654, 718_{sh}	34.7	0.21
2A	CH_2Cl_2[a](77)	362	471_{max}, 506, 547, 593_{sh}	541.0	
	CH_2Cl_2[b] (77)	367	475_{max}, 509, 552, 603_{sh}	435.3	
	CH_2Cl_2[b] (77)	400	475, 509, 567_{max}, 612, 663_{sh}	73.9	
	PMMA Film	340	476_{max}, 510, 550, 597_{sh}		0.53
	Solid (298)	361	560, 601_{max}, 649	47.4	0.24
3A	CH_2Cl_2[a](77)	363	473_{max}, 508, 548, 594_{sh}	563.9	
	CH_2Cl_2[b] (77)	373	475_{max}, 510, 552, 603_{sh}	419.0	
		395	475, 510, 570_{max}, 617, 669_{sh}	110.4	
	PMMA Film	340	476_{max}, 511, 551, 598_{sh}		0.89
	Solid (298)	375	476, 510, 578_{max}, 613		0.06
		400	476, 510, 582, 615_{max}	21.8	
1B	CH_2Cl_2[a](77)	324	464, 493_{max}, 525, 565_{sh}	19.2	
	CH_2Cl_2[b] (77)	365	469_{max}, 500, 531, 570_{sh}	23.5	
	PMMA Film	340	463, 491_{max}, 519, 560_{sh}		0.74
	Solid (298)	367	473, 497_{max}, 529	13.3	0.37
2B	CH_2Cl_2[a](77)	320	449_{max}, 479, 511, 545_{sh}	25.6	
	CH_2Cl_2[b] (77)	348	456_{max}, 486, 517, 552_{sh}	25.0	
	PMMA Film	330	453, 481_{max}, 506, 546_{sh}		0.62
	Solid (298)	373	467_{sh}, 489_{max}, 514_{sh}, 558_{sh}	4.2	0.10
3B	CH_2Cl_2[a](77)	327	455_{max}, 487, 516, 553_{sh}	23.9	
	CH_2Cl_2[b] (77)	350	456_{max}, 488, 518, 557_{sh}	22.4	
	PMMA Film	330	453, 481_{max}, 506, 546_{sh}		0.95
	Solid (298)	361	463, 484_{max}, 510	18.0	0.40

a = 10^{-5} M; *b* = 10^{-3} M; *c*= data at λ_{max}; *d* = 5 wt% PMMA films in Ar atmosphere.

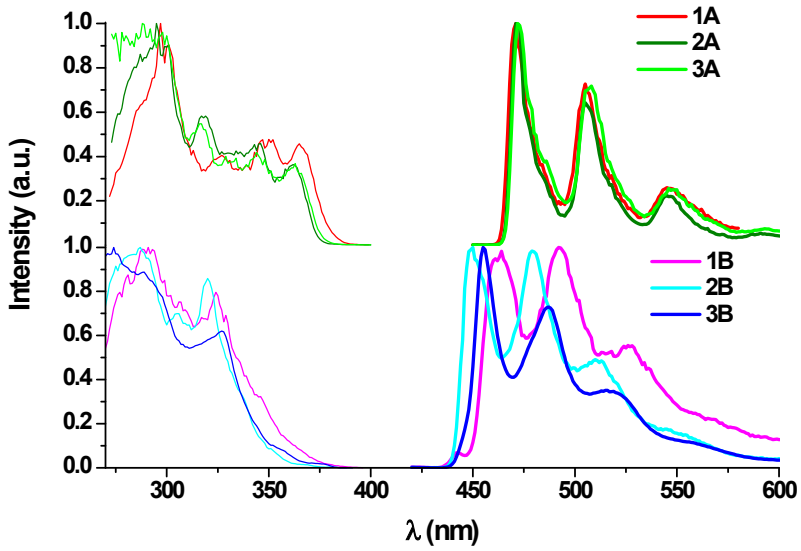

Figure S12. Normalized excitation and emission spectra of **1A–3A** and **1B–3B** at 77 K in rigid matrix of CH_2Cl_2 (10^{-5} M).

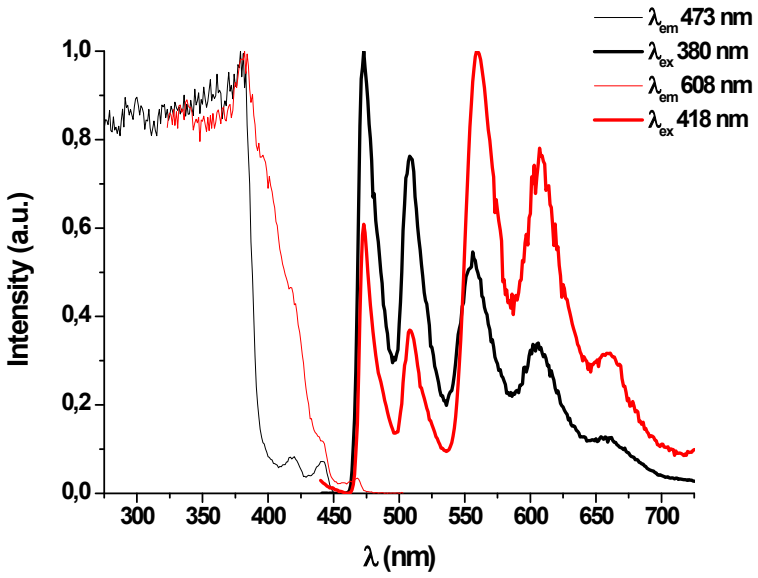

Figure S13. Normalized excitation and emission spectra of **1A** in rigid matrix of CH_2Cl_2 (10^{-3} M, 77 K).

7. Devices performance and Characteristics

7.1 OLEDs

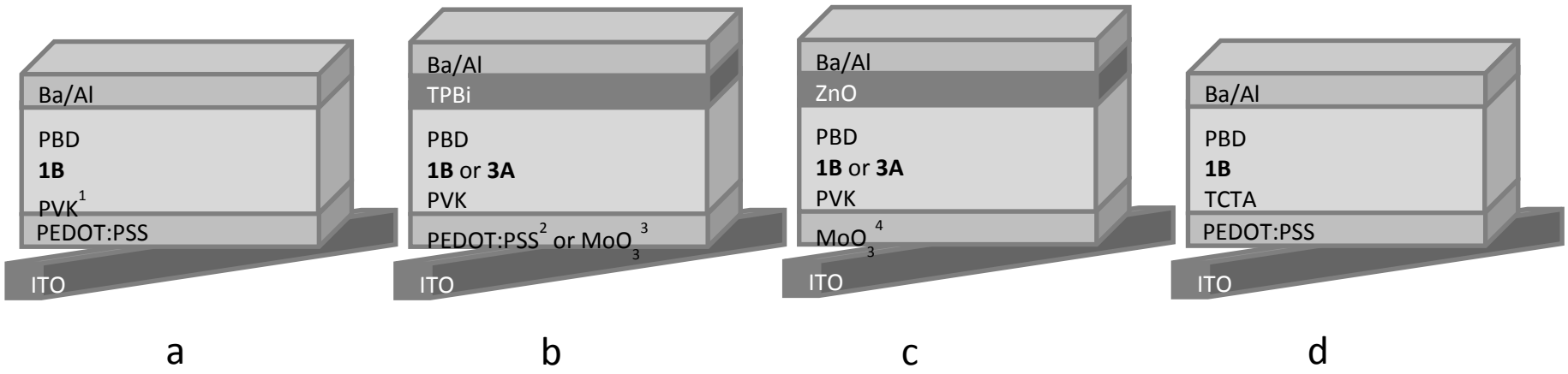

Figure S14. Device architectures of monochromatic OLEDs: **L1-L9** (a,b,c) and **OL1-OL3** (d),

Table S11. Emiting layer composition and EQE of **L1-L9**.

	EML (%)	**HTL**	**ETL**	**EQE**
L1	**1B** (10)	63	27	0.1
L2	**1B** (15)	59	26	<0.01
L3	**1B** (20)	57	23	0.02
L4	**1B** (10)	63	27	0.1
L5	**1B** (10)	63	27	0.12
L6	**1B** (10)	63	27	0.08
L7	**3A** (10)	63	27	0.3
L8	**3A** (10)	63	27	0.4
L9	**3A** (10)	63	27	0.015
OL1	**1B** (5)	47.5	47.5	0.02
OL2	**1B** (10)	45	45	0.02
OL3	**1B** (20)	40	40	0.02

First of all, we built OLEDs containing **1B** or **3A** as emitters, to optimize the operating conditions for each of them (see Table S11 and Figures S14a, b, c and S15a, b, c). We followed the host-guest approach typical of phosphorescent emitters by dispersing the **1B** and **3A** compounds in a two-components bipolar host based on polyvinylcarbazole (PVK) and 2-(4-tert-Butylphenyl) -5-(4-biphenylyl)-1,3,4-oxadiazole (PBD) as hole and electron transporting compounds, respectively. The choice of PVK relies on both its good hole transport properties and its suitable LUMO energy level with respect to that of **1B** (- 2.13 eV, Table S8 in SI) that blocks electron flow toward anode and help in confining excitons within the active layer. The T_1 energy of PVK is lower than the one of **1B**, that could create non radiative recombination pathways, but the test of alternative compounds like TCTA, featuring an higher T_1, resulted in a TCTA:**1B** green electroplex emission[20] and very low EQE (see SI, Figures S14d and 15d and Table S11, OL1-OL3).

Devices **L1-L3** were initially prepared with a simple ITO/PEDOT:PSS/PVK:PBD:**1B**/Ba/Al configuration (see Figure S14a), where a solution of the blend in $CHCl_3$ was deposited by spin-coating with different **1B** doping concentrations (see Table S11).

The electroluminescent (EL) spectra of **L1-L3**, as can be observed in Figure S15 a, are dominated by Pt(II) complex emission. However, a weak contribution of PVK emission (λ_{max} ~ 420 nm) to the EL is detected in the device with the lowest content of **1B** (**L1**). The concentration study **L1-L3** ranging from 10-to-20 wt% reveals that, although higher concentrations prevent the emission of PVK, emission quenching due to aggregation affects the EQE. Thus, 10 wt% was found to be the most appropriate doping concentration.

Devices **L4-L6** with fixed 10 wt% **1B** content in the EML and improved charge injection regulation and exciton confinement were prepared and tested (see Figures S14 b-c and Table S11) with the aim of enhance EQE and suppress PVK contribution. The integration of vacuum growth TPBi thin film (20 nm) as electron injection layer (EIL) (**L4**), and the substitution of PEDOT:PSS by MoO_3 (10 nm) (**L5)** (Figures S14b-c), with a much lower work function (-6.69 eV) to improve the hole injection, were evaluated. No EQE enhancement was achieved, but a progressive reduction of PVK contribution in EL spectra (Figure S15b), dominated by **1B** emission, was observed going from device **L3** to **L5**. Further, the integration of a solution processed ZnO film (**L6**) as EIL instead of TPBI, that acts as a better hole-blocking layer thanks to a deep

HOMO orbital (-7.0 eV), totally suppressed PVK contribution by exciton confinement within the EML.

Devices **L7**-**L9** containing **3A** orange emitter in the EML, were prepared with the same architectures of **L4**-**L6** devices, respectively, and using a blend of PVK and PBD as host material (see Figures S14b,c, S15c and Table S11). The broad emission of **3A** at high doping concentration could be exploited in term of improved CRI, so **3A** concentration is varied in the EML. The EQE of **L7** is considerably higher than its blue homologous **L4**, but is still modest, which can be understood once considered that also **3A** features a very deep HOMO (Table S8 in ESI). The EL spectrum of **L7** (see Figure S15 c) shows three main contributions: the blue emission from PVK (λ_{max} ~ 420 nm), yellow structured band (λ ~ 477, 510 nm) corresponding to the HE emission of **3A** (Figure 4) and a major contribution corresponding to the LE emission band of **3A**. As in the case of **1B**-based OLEDs, in order to reduce the PVK contribution, PEDOT:PSS was substituted by MoO_3 (**L8**). The intensity of the PVK band was reduced by half, thus obtaining **3A** LE and HE emission with slightly higher EQE (see Table S11). Moreover, the insertion of a ZnO film as EIL (**L9**) increases the contribution of the HE band with respect to LE one, but severely affects the EQE (see Table S11 and Figure S15c).

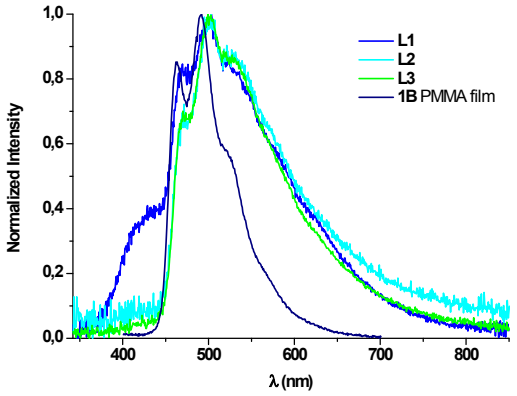

(a)

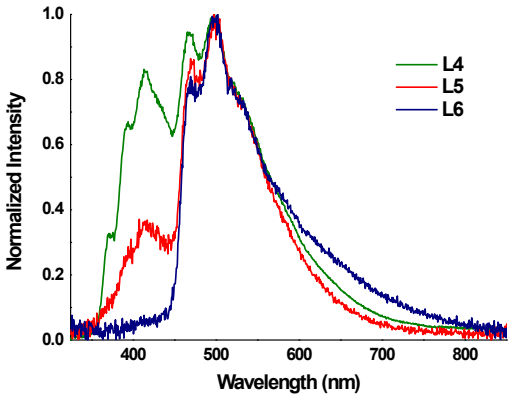

(b)

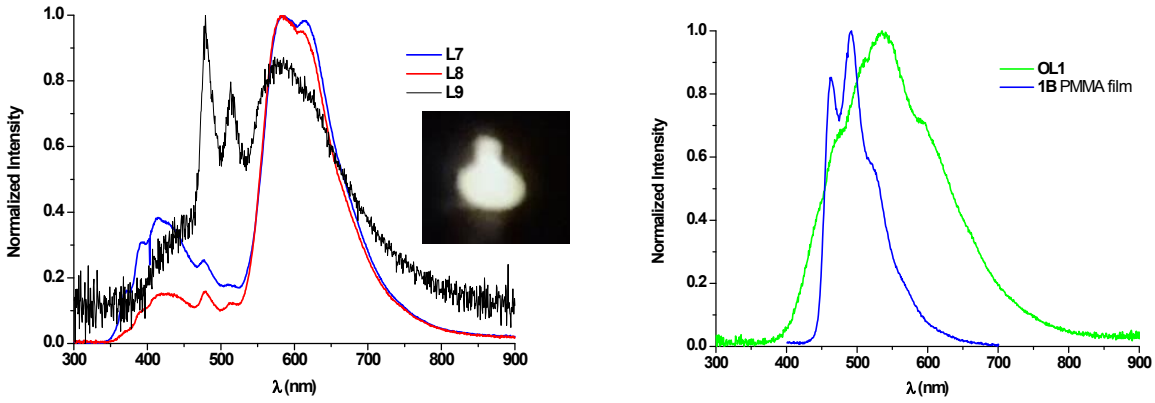

(c) **(d)**

Figure S15. EL spectra of devices **L1-L9** driven at 10 V; picture of working **L8** device EL spectrum of **OL1** (d) compared to the PL spectrum of **1B** in PMMA

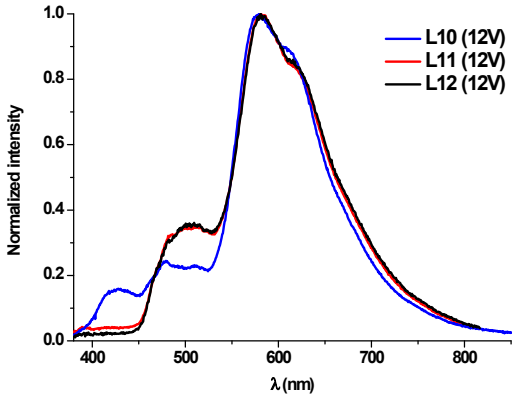

Figure S16. Electroluminescence of devices **L10-L12** at 12V

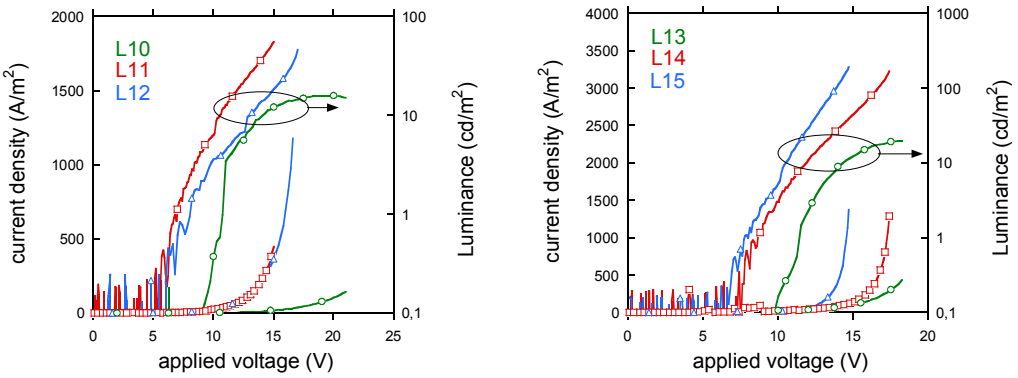

(a) (b)

Figure S17. Current density-voltage-luminance (J-V-L) curves of **L10-12** (a) and **L13-15** (b).

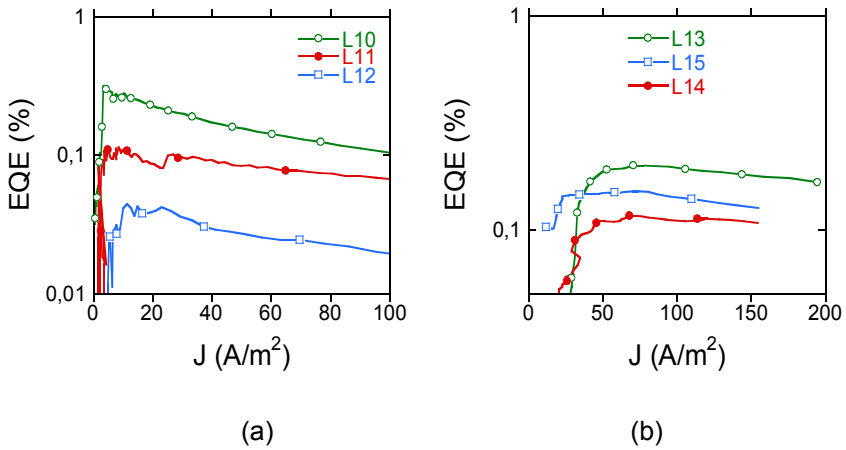

Figure S18. EQE versus J curves of **L10-12** (a) and **L13-15** (b).

7.2 Remote-phosphors

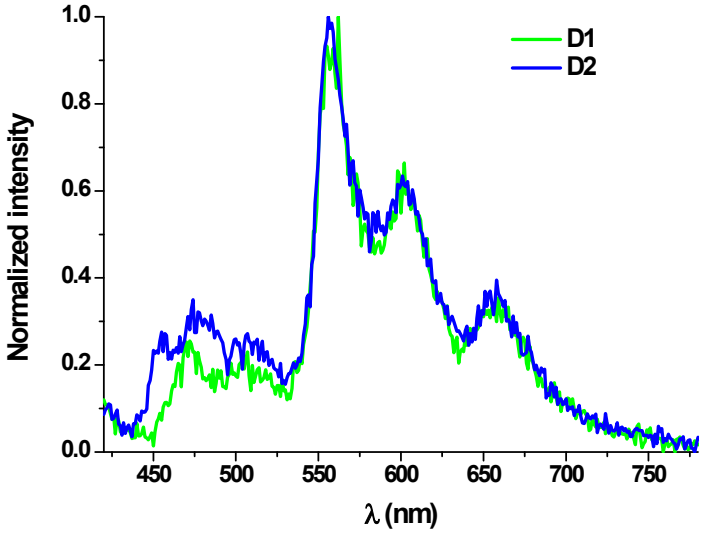

Figure S19. Normalized emission spectra of **D1** and **D2**

References

1. C. c. d. r. p. CrysAlis RED, Oxford Diffraction, 2006.
2. G. M. Sheldrick, *Acta Crystallographica Section A*, 2008, **64**, 112-122.
3. L. Farrugia, *J. App. Crystallogr.*, 1999, **32**, 837-838.
4. A. L. Spek, *Acta Cryst.* , 2009, **D65**, 148-155.
5. Y. Zhao and D. G. Truhlar, *Theor. Chem. Acc.*, 2008, **120**, 215-241.
6. M. J. Frisch, G. W. Trucks, H. B. Schlegel, G. E. Scuseria, M. A. Robb, J. R. Cheeseman, G. Scalmani, V. Barone, B. Mennucci, G. A. Petersson, H. Nakatsuji, M. Caricato, X. Li, H. P. Hratchian, A. F. Izmaylov, J. Bloino, G. Zheng, J. L. Sonnenberg, M. Hada, M. Ehara, K. Toyota, R. Fukuda, J. Hasegawa, M. Ishida, T. Nakajima, Y. Honda, O. Kitao, H. Nakai, T. Vreven, J. A. Montgomery Jr., J. E. Peralta, F. Ogliaro, M. J. Bearpark, J. Heyd, E. N. Brothers, K. N. Kudin, V. N. Staroverov, R. Kobayashi, J. Normand, K. Raghavachari, A. P. Rendell, J. C. Burant, S. S. Iyengar, J. Tomasi, M. Cossi, N. Rega, N. J. Millam, M. Klene, J. E. Knox, J. B. Cross, V. Bakken, C. Adamo, J. Jaramillo, R. Gomperts, R. E. Stratmann, O. Yazyev, A. J. Austin, R. Cammi, C. Pomelli, J. W. Ochterski, R. L. Martin, K. Morokuma, V. G. Zakrzewski, G. A. Voth, P. Salvador, J. J. Dannenberg, S. Dapprich, A. D. Daniels, Ö. Farkas, J. B. Foresman, J. V. Ortiz, J. Cioslowski and D. J. Fox, *Journal*, 2009.
7. D. Andrae, U. Haussermann, M. Dolg, H. Stoll and H. Preuss, *Theor. Chim. Acta*, 1990, **77**, 123-141.
8. R. Ditchfield, W. J. Hehre and J. A. Pople, *J. Chem. Phys.*, 1971, **54**, 724-728.
9. Harihara.Pc and J. A. Pople, *Theor. Chim. Acta*, 1973, **28**, 213-222.
10. U. Varetto and M. S. N. S. C. L. (Switzerland), 2009.
11. S. Fuertes, A. J. Chueca, M. Perálvarez, P. Borja, M. Torrell, J. Carreras and V. Sicilia, *ACS App. Mat. Interfaces*, 2016, **8**, 16160-16169.
12. S. Fuertes, A. J. Chueca and V. Sicilia, *Inorg. Chem.*, 2015, **54**, 9885-9895.
13. S. Fuertes, H. Garcia, M. Peralvarez, W. Hertog, J. Carreras and V. Sicilia, *Chem. - Eur. J.*, 2015, **21**, 1620-1631.
14. Y. Unger, D. Meyer, O. Molt, C. Schildknecht, I. Münster, G. Wagenblast and T. Strassner, *Angew. Chem., Int. Ed.*, 2010, **49**, 10214-10216.
15. Z. M. Hudson, C. Sun, M. G. Helander, Y. L. Chang, Z. H. Lu and S. N. Wang, *J. Am. Chem. Soc.*, 2012, **134**, 13930-13933.
16. A. Diez, J. Fornies, S. Fuertes, E. Lalinde, C. Larraz, J. A. Lopez, A. Martin, M. T. Moreno and V. Sicilia, *Organometallics*, 2009, **28**, 1705-1718.
17. S. Graber, K. Doyle, M. Neuburger, C. E. Housecroft, E. C. Constable, R. D. Costa, E. Orti, D. Repetto and H. J. Bolink, *J Am Chem Soc*, 2008, **130**, 14944-14945.
18. H. Jude, F. N. Rein, P. S. White, D. M. Dattelbaum and R. C. Rocha, *Inorg Chem*, 2008, **47**, 7695-7702.
19. W. J. Geary, *Coordin Chem Rev*, 1971, **7**, 81-122.
20. D. Das, P. Gopikrishna, R. Narasimhan, A. Singh, A. Dey and P. K. Iyer, *Phys. Chem. Chem. Phys.*, 2016, **18**, 33077-33084.